


Received December 27, 2021, accepted January 9, 2022, date of publication January 25, 2022, date of current version February 2, 2022.

Digital Object Identifier 10.1109/ACCESS.2022.3146075

2D Direction of Arrival Estimation Using Uniform Circular Arrays With Radiation Pattern Reconfigurable Antennas

BRAD R. JACKSON , (Senior Member, IEEE)

Department of Electrical and Computer Engineering, California State University, Northridge, CA 91330, USA

e-mail: brad.jackson@csun.edu


ABSTRACT This paper focuses on direction of arrival (DoA) estimation using adaptive arrays that consist of radiation pattern reconfigurable antenna (RPRA) elements for 2D direction finding (i.e., azimuth and elevation DoA estimation). In particular, uniform circular arrays (UCAs) are explored that use RPRA elements with two different elevation radiation pattern states to achieve unambiguous estimates over all possible incident angles. Theoretical cardioid-type directional patterns are investigated to determine the pattern states that minimize overall DoA estimation error, and the performance of 3-, 4-, and 5-element RPRA UCAs is compared with baseline theoretical arrays composed of isotropic elements. The results demonstrate that RPRA UCAs with optimized cardioid patterns can achieve similar accuracy to the baseline arrays, but with fewer antennas/front-ends. For example, a 4-element RPRA UCA can achieve approximately the same root mean square error (RMSE) as a 6-element uniform spherical array composed of isotropic elements. Furthermore, unambiguous estimates can be achieved over all incident angles with electrically large UCA radii using optimized RPRA elements, which can further improve accuracy and increase bandwidth. To demonstrate the feasibility of the technique, a practical RPRA was designed at 6 GHz with a pattern that approximates the optimized cardioid, and the performance meets or exceeds the theoretical pattern performance for RMSEs less than 3° .

INDEX TERMS 2D direction of arrival estimation, direction finding, radiation pattern reconfigurable antennas, multifunction reconfigurable antenna arrays, adaptive arrays, smart antennas.

I. INTRODUCTION

The ability to accurately determine an incident signal's direction of arrival (DoA) is critical for a wide range of commercial and military applications. For example, the estimated DoA of an incident radio frequency (RF) signal can be used for beamforming/nullforming in an adaptive array for modern wireless communications systems, or this information could be used as part of electronic warfare operations.

Depending on the application, it may only be necessary to estimate the DoA in one plane (i.e., an estimate of either the azimuth angle, ϕ , or the elevation angle, θ , but not both simultaneously). Such a 1-dimensional (1D) DoA estimation can be useful in terrestrial applications where both the transmitter and receiver are at the same elevation. However,

The associate editor coordinating the review of this manuscript and approving it for publication was Tutku Karacolak .

in applications where the transmitter and receiver may be in any relative position, 2D DoA estimation must be performed to obtain estimates for both the elevation and azimuth angles of arrival, (θ, ϕ) . For example, 2D DoA estimation is suitable for aerospace applications where the incident signal may be from any relative direction in 3D space.

There are a variety of array geometries that are often used to perform DoA estimation. These include uniform linear arrays (ULAs), uniform rectangular arrays (URAs), uniform circular arrays (UCAs), uniform cylindrical arrays (UCylAs), and uniform spherical arrays (USphAs). The array geometry has a direct impact on the accuracy of the DoA estimation, as well as the angles over which DoA estimation is reliable and ambiguity-free. Ambiguities in DoA estimation occur when multiple incident signal directions produce the same excitations of the antenna elements, potentially resulting in large estimation errors. UCAs are often used for DoA estimation to potentially provide uniform accuracy across all

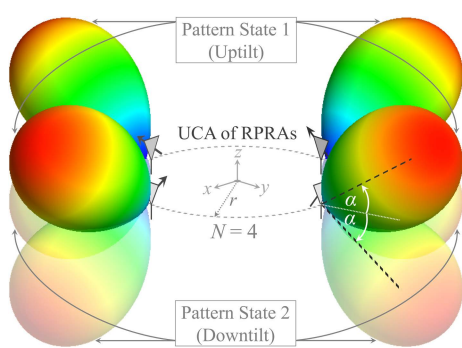


FIGURE 1. Concept for employing RPR elements in a UCA for 2D DoA estimation. An $N = 4$ element UCA with radius r is illustrated where each element is an RPR that has two potential directional radiation pattern states: (i) an uptilt state directed at an angle α above the plane of the array, and (ii) a downtilt state directed at an angle α below the plane of the array.

incident angles in the plane of the array. However, since the elements in a UCA are in one plane, this type of array is not typically well-suited to 2D direction finding and can result in ambiguous DoA estimates in elevation angle if the full sphere of possible incident angles is considered ($0^\circ \leq \theta \leq 180^\circ$, $0^\circ \leq \phi < 360^\circ$).

The focus of this paper is on the use of reconfigurable antennas as the elements in a UCA to enable unambiguous direction finding over all 3D space, particularly for applications with constrained size, weight, and power (SWaP). Reconfigurable antennas can have their characteristics dynamically altered including their radiation pattern, frequency response, and/or polarization. There are a variety of mechanisms that can be used to control the state of a reconfigurable antenna such as PIN diode switches, RF MEMS switches, and varactors (e.g., see [1], [2] for an overview). Shown in Fig. 1 is the concept explored in this work where an $N = 4$ element UCA is illustrated that consists of radiation pattern reconfigurable antenna (RPR) elements, each of which has two potential radiation pattern states: (i) an uptilt state directed at an angle α above the plane of the array, and (ii) a downtilt state directed at an angle α below the plane of the array.

Adaptive arrays typically require an independent receiver channel for each antenna element that consists of an RF front-end (e.g., filters, amplifiers, mixers, local oscillators, etc.), and an analog-to-digital converter (ADC). Each channel can consume significant power, which can limit the application of adaptive arrays on SWaP-constrained platforms such as small unmanned aerial vehicles (UAVs) and small satellites [3]. The work presented in this paper focuses on combining RPRAs with the inherent advantages of adaptive arrays in order to achieve unambiguous 2D DoA estimation. If the use of RPRAs can enable acceptable performance with fewer receiver channels compared to conventional elements, then the SWaP and cost of the system could potentially be significantly reduced and new applications could be enabled.

The background and contributions of the paper are discussed in Section II, and the DoA system model is detailed in

Section III. Following this, the performance and optimization of UCAs using RPRAs with theoretical cardioid patterns is explored in Section IV, as well as a comparison with baseline arrays consisting of isotropic non-reconfigurable elements. Section V presents the design and simulation results of a practical RPR, and lastly, conclusions are discussed in Section VI.

II. BACKGROUND AND CONTRIBUTIONS

The prior work most relevant to this paper can be categorized as (i) DoA estimation performance improvement through antenna element/array optimization, and (ii) DoA estimation using reconfigurable antennas. The first category is fairly extensive given the long history of direction finding (DF). Recent efforts have investigated various antenna array geometries [4]–[7] and the effect of the antenna element itself [8]–[15] in order to improve DoA estimation performance. In particular, the use of directive antennas as the array elements has been a focus in many of these works. The orientation of the directive antenna elements in various array configurations was explored in [7]–[11] which can lead to improved DoA estimation accuracy. In [12], the dependence of antenna element directivity in UCAs was investigated, and it showed the potential 1D (azimuth-only) DoA estimation performance improvement that can be achieved through optimizing the antenna elements. Further studies on non-reconfigurable directive elements have included truncated hexagonal pyramid [7] and cylindrical [13] conformal arrays that are capable of 2D DoA estimation (i.e., azimuth and elevation angles).

While the vast majority of prior work on DoA estimation with adaptive arrays has focused on fixed non-reconfigurable antennas, there have been a number of investigations on the use of reconfigurable elements [16]–[33]. In [16], a UCA was composed of 8 parasitic layer-based multifunctional reconfigurable antenna (MRA) elements. In this work, a computationally efficient iterative mode selection technique was used to select between 25 different element states, which showed improved DoA performance compared to a UCA composed of dipole elements. A similar approach was also used in an earlier work [17] where a planar rectangular array was studied using parasitic layer reconfigurable antenna elements that focused on a spatial smoothing technique to improve DoA performance. These papers did not explore the impact of element directivity on 2D DoA estimation performance. In [18]–[20], reconfigurable adaptive antenna arrays were considered that have more antenna elements than front-ends available, thus necessitating the selection of a subset of elements to form the optimum subarray. These papers showed significant performance preservation while minimizing the hardware required, but the focus was not on the optimization of radiation pattern states of RPRAs for DoA estimation.

Composite right/left handed (CRLH) leaky-wave antennas (LWAs) have been used as reconfigurable antenna elements to control the radiation pattern and estimate the

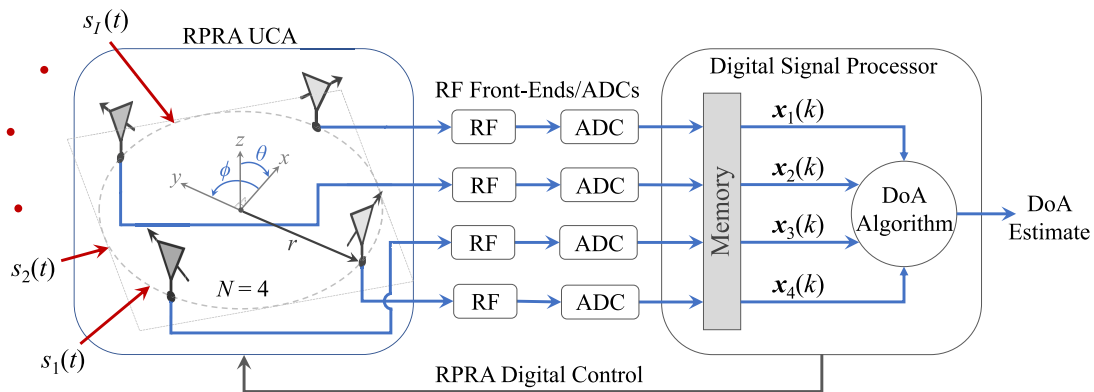


FIGURE 2. System diagram for DoA estimation using a UCA composed of $N = 4$ radiation pattern reconfigurable antenna elements.

DoA using a single antenna in several works [21]–[26]. The radiation pattern of the CRLH LWA can be scanned throughout one plane by controlling the DC bias of varactor diodes. Multiple CRLH LWAs at different locations were used in [21]–[23] to perform DoA estimation, but not in a uniform array configuration. Only planar 1D DoA estimation was considered in these papers and the optimization of the radiation pattern states is not discussed.

RF switches were used to control the radiation patterns in [28]–[30] to perform DoA estimation. In [28], a reconfigurable switched-beam antenna that can generate 11 figure-eight-shaped radiation patterns was electronically rotated in the azimuth plane to perform DF with a single-channel amplitude-only receiver. RSS systems have the inherent advantage of low-complexity receivers; however, the resulting accuracy will generally be reduced compared to a DoA estimation system that also uses phase information.

This work explores the use of elevation pattern diversity in RPRU elements to achieve unambiguous 2D DoA estimation with UCAs over all angles $0^\circ \leq \theta \leq 180^\circ$, $0^\circ \leq \phi < 360^\circ$. The overall goal is to optimize DoA estimation performance for low numbers of independent channels in an adaptive array receiver ($N \leq 5$). The use of a planar 2D UCA geometry could be advantageous for installations on aerospace platforms (e.g., around the fuselage of a UAV or on four sides of a CubeSat). To minimize the complexity of the RPRU element design, two-state RPRUs with cardioid-type patterns are studied, and the theoretical radiation pattern characteristics that minimize overall DoA estimation error are identified. Once the desired radiation patterns are determined, the resulting DoA estimation performance is compared with baseline theoretical arrays composed of isotropic elements, and a practical RPRU design is explored in an attempt to closely approximate the ideal theoretical cardioid pattern.

The specific contributions of this paper include:

- (i) The first UCA design using RPRUs that demonstrates unambiguous DOA estimation over the full sphere of incident angles.

- (ii) The first systematic and detailed investigation into the optimization of RPRU array elements for 2D DoA estimation.
- (iii) The first comparison of 2D DoA estimation performance of UCAs that use RPRUs with baseline theoretical arrays that use isotropic antenna elements.
- (iv) The first practical RPRU design that has been optimized to minimize 2D DoA estimation error.

III. DoA SYSTEM MODEL

A. RECEIVER MODEL FOR UCAs WITH RPRUs

A high-level system diagram of the proposed adaptive UCA consisting of reconfigurable antenna elements for DoA estimation is shown in Fig. 2. This diagram shows four RPRUs, where the pattern state of each is determined by a digital control signal. With the RPRUs in State 1 (e.g., the uptilt state in Fig. 1), I incoming RF signals, $s_i(t)$, are received by the array from incident angles (θ_i, ϕ_i) , $i = 1 \dots I$. Separate RF front-ends then perform filtering, amplification, and frequency conversion, prior to discretizing the signal via analog-to-digital converters. The ADCs produce K samples of the received signal from each of the four elements, which are stored in memory. The digital control signal then changes the radiation pattern state of each RPRU to State 2 (e.g., the downtilt state in Fig. 1) and an additional K samples of the received signal are taken and stored in memory, resulting in a total of $2K$ samples for each element. This process could continue for more RPRU states, but for simplicity and to limit the sampling period duration (or alternatively, to limit the deleterious effects of a reduced sampling period in each state), this paper only considers the case where the RPRUs are switched between two patterns. For a practical implementation, switching speed is an important consideration. Solid state switches can have speeds on the order of nanoseconds whereas RF MEMS switches typically have speeds on the order of microseconds. In this work, for generality and to investigate the concept, ideal switches are used.

It is assumed that the DoA of the incident signal does not change over the sampling period. To illustrate this assumption, consider 4G LTE cellular which has a sampling rate of 30.72 MHz for a 20 MHz system bandwidth. If 100 total samples are used (which is the number used later in this paper), the total sampling period would be 3.26 μ s. Over this short period of time, the incident signal angle would not change significantly unless the transmitter is moving at a very high speed relative to the receiver. It is also assumed that the symbol duration is much longer than the total sampling period.

Capturing K samples in each of the two pattern states requires twice the total sampling period compared to a traditional adaptive array using non-reconfigurable elements, and is a potential disadvantage of this technique. For a fair evaluation, the performance comparisons discussed later in the paper use $2K$ samples for the conventional adaptive arrays using fixed theoretical isotropic antenna elements (i.e., an equal total sampling period).

With reference to Fig. 1 and Fig. 2, the received complex samples in each state for N antenna elements are given by:

$$\mathbf{x}^u(k) = \begin{bmatrix} x_1^u(k) \\ x_2^u(k) \\ \vdots \\ x_N^u(k) \end{bmatrix} \quad \mathbf{x}^d(k) = \begin{bmatrix} x_1^d(k) \\ x_2^d(k) \\ \vdots \\ x_N^d(k) \end{bmatrix}, \quad (1)$$

where \mathbf{x}^u represents the up-tilt state, \mathbf{x}^d represents the down-tilt state, and $k = 1 \dots K$ is the sample index, which restarts at $k = 1$ when the RPRA switches states. Signal sample alignment across the two pattern states can be achieved using knowledge of the signal frequency, the sampling period, and the number of samples. Since the samples are stored in memory and time-invariance over the sampling period is assumed, they can be combined and processed together (i.e., as if the array consisted of $2N$ separate non-reconfigurable antenna elements that receive the signal concurrently),

$$\begin{aligned} \mathbf{x}_1(k) &= [x_1^u(k) \ x_1^d(k)] \\ \mathbf{x}_2(k) &= [x_2^u(k) \ x_2^d(k)] \\ &\vdots \\ \mathbf{x}_N(k) &= [x_N^u(k) \ x_N^d(k)] \end{aligned} \quad (2)$$

$$\mathbf{x}(k) = [\mathbf{x}_1(k) \ \mathbf{x}_2(k) \ \dots \ \mathbf{x}_N(k)]^T, \quad (3)$$

where T is the transpose operator. The array response vector (ARV), also known as the steering vector, is given by:

$$\mathbf{a}(\theta, \phi) = \begin{bmatrix} g_1^u(\theta, \phi)e^{j\psi_1(\theta, \phi)} \\ g_1^d(\theta, \phi)e^{j\psi_1(\theta, \phi)} \\ g_2^u(\theta, \phi)e^{j\psi_2(\theta, \phi)} \\ g_2^d(\theta, \phi)e^{j\psi_2(\theta, \phi)} \\ \vdots \\ g_N^u(\theta, \phi)e^{j\psi_N(\theta, \phi)} \\ g_N^d(\theta, \phi)e^{j\psi_N(\theta, \phi)} \end{bmatrix}, \quad (4)$$

where $g_n^{u/d}(\theta, \phi)$, $n = 1, 2, \dots, N$ represent the gains of the antenna up-tilt/down-tilt states in the (θ, ϕ) direction. The phase shift at each element is determined by:

$$\psi_n(\theta, \phi) = \frac{2\pi}{\lambda} (x_n \sin \theta \cos \phi + y_n \sin \theta \sin \phi), \quad (5)$$

where λ is the wavelength. The x - y Cartesian coordinates of the RPRA elements in a UCA with radius r are $x_n = r \cos(\frac{2\pi(n-1)}{N})$ and $y_n = r \sin(\frac{2\pi(n-1)}{N})$ with the UCA oriented in the x - y plane.

Prior to the use of a practical reconfigurable antenna implementation discussed later in this paper, the N RPRA elements in the UCA will be treated as rotated versions of a theoretical base radiation pattern that will be detailed in the next subsection. Note that the ARV elements represent the magnitude and phase of a received signal from a particular direction, and as such, the gain terms in (4), $g_n^{u/d}(\theta, \phi)$, can be thought of as a voltage or current gain, which is the square root of the antenna's power pattern, $G_n^{u/d}(\theta, \phi)$.

The matrix of steering vectors due to I incident signals is:

$$\mathbf{A} = [\mathbf{a}(\theta_1, \phi_1) \ \mathbf{a}(\theta_2, \phi_2) \ \dots \ \mathbf{a}(\theta_I, \phi_I)], \quad (6)$$

and the received signal at the antenna elements is:

$$\mathbf{x}(k) = \mathbf{A} \cdot \mathbf{s}(k) + \boldsymbol{\eta}(k), \quad (7)$$

where $\mathbf{s}(k) = [s_1(k) \ s_2(k) \ \dots \ s_I(k)]^T$ are the discretized incoming signals at sample k , and the noise is represented by $\boldsymbol{\eta}(k)$ which is a complex-valued zero-mean circular Gaussian random vector. The noise contributions are assumed to be from (i) the RF front-ends, each of which is assumed to have equal noise variance, and (ii) from spatially-uniform noise that is sensed from the environment. To generate the noise in numerical simulations, zero-mean complex Gaussian noise was added to each sample with variance corresponding to the desired signal-to-noise ratio (SNR).

The multiple signal classification (MUSIC) algorithm [34] is a commonly-used method to estimate the DoA in adaptive arrays (e.g., it was used to evaluate performance in [7], [10], [13], [14], [17], [21], [25]–[27]). The MUSIC algorithm, which is based on the eigenvalue decomposition of the array covariance matrix, is also the method that was used to evaluate and compare DoA estimation performance in this work. This algorithm has been used with reconfigurable antennas previously in a manner that is similar to how it is used in this paper (i.e., by considering the pattern states as if they are separate antennas receiving the incident signal concurrently) [26]. The time-averaged array correlation matrix of $\mathbf{x}(k)$ assuming ergodicity is given by:

$$\mathbf{R}_{\mathbf{xx}} = \frac{1}{K} \sum_{k=0}^{K-1} \mathbf{x}(k)\mathbf{x}^H(k), \quad (8)$$

where $(\cdot)^H$ denotes the Hermitian transpose. The 2D MUSIC algorithm generates a DoA-dependent pseudospectrum that is calculated with:

$$P(\theta, \phi) = \frac{1}{\Lambda_{\min} \left(\begin{bmatrix} \mathbf{a}_\theta^H(\theta, \phi) \\ \mathbf{a}_\phi^H(\theta, \phi) \end{bmatrix} \mathbf{E}_N \mathbf{E}_N^H \begin{bmatrix} \mathbf{a}_\theta(\theta, \phi) \\ \mathbf{a}_\phi(\theta, \phi) \end{bmatrix} \right)}, \quad (9)$$

where $\Lambda_{\min}(\cdot)$ represents the minimum eigenvalue, $\mathbf{a}_\theta(\theta, \phi)$ and $\mathbf{a}_\phi(\theta, \phi)$ are the ARVs separated by wavefront polarization, and \mathbf{E}_N represents the noise eigenvectors of $\mathbf{R}_{\mathbf{x}\mathbf{x}}$. The resulting $P(\theta, \phi)$ will exhibit peaks for angles where the incident signal's ARV is orthogonal to the noise subspace. Thus, upon calculating the pseudospectrum, a peak search can be performed over all (θ, ϕ) to estimate the 2D DoA of the incident signal(s).

B. THEORETICAL RECONFIGURABLE ELEMENT PATTERNS

In order to determine the DoA estimation performance of a UCA composed of reconfigurable elements, the specific radiation pattern states of the RPRAs must be known. Intuitively, the pattern shape and directivity of the RPRAs along with their tilt angle, α , will have a significant impact on DoA estimation performance. Since the practical design of numerous RPRAs with varying patterns and tilt angles would be extremely time-consuming, a mathematical model for the radiation pattern was used to analyze performance. Once the theoretical radiation patterns with the best performance are identified, a practical RPRAs design can be implemented to approximate the desired patterns. Since there are an infinite number of potential radiation patterns, some of which would be impractical to realize with an actual antenna design, the analysis was limited to a specific family of radiation patterns that can potentially be approximated with realizable antennas. Specifically, cardioid-type symmetrical radiation patterns were considered based on:

$$\hat{U}(\theta, \phi) = \frac{1}{2^\rho} (1 + \cos \theta)^\rho \tag{10}$$

where ρ determines the maximum directivity, D , and the division by 2^ρ is for normalization. The antenna gain as a function of angle, assuming the antenna is lossless, is given by $\hat{G}(\theta, \phi) = D\hat{U}(\theta, \phi)$. The focus on this family of theoretical unidirectional radiation patterns is motivated by the wide variety of different types of antennas that have been demonstrated to exhibit cardioid-type patterns such as rectangular patches [12], circular patches [35], dielectric resonator antennas [36], and Huygens antennas [37]. The diversity of antennas that can produce this pattern type could potentially provide flexibility in the antenna element implementation. Furthermore, its directivity and pointing angle are easily mathematically adjusted and it can potentially model the back-side radiation present in antennas with small ground planes.

The theoretical RPRAs of interest in this paper are those that have two potential radiation pattern states: one with an elevation uptilt, and one with an elevation downtilt, with the patterns directed away from the center of the UCA (see Fig. 1). In order to achieve this, the base theoretical radiation pattern can be rotated in both elevation and azimuth angles. A straight-forward way to achieve this rotation is to first transform from the spherical coordinate system to Cartesian, $\hat{G}(\theta, \phi) \rightarrow (\hat{G}_x, \hat{G}_y, \hat{G}_z)$. Then, a rotation around the y -axis followed by a rotation around the z -axis can be performed

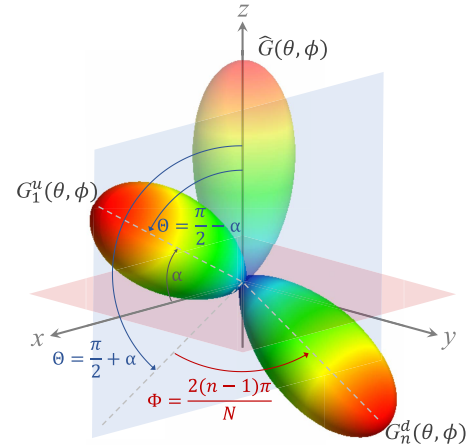


FIGURE 3. Radiation pattern rotation illustrating the base radiation pattern, $\hat{G}(\theta, \phi)$, rotated in elevation to form an uptilt state $\hat{G}_1^u(\theta, \phi)$. Also shown is a generalized downtilt state for the n^{th} antenna element, $\hat{G}_n^d(\theta, \phi)$, that has been rotated in both elevation and azimuth.

using the following rotation matrices:

$$\mathbf{R}_y(\Theta) = \begin{bmatrix} \cos \Theta & 0 & \sin \Theta \\ 0 & 1 & 0 \\ -\sin \Theta & 0 & \cos \Theta \end{bmatrix}, \tag{11}$$

$$\mathbf{R}_z(\Phi) = \begin{bmatrix} \cos \Phi & -\sin \Phi & 0 \\ \sin \Phi & \cos \Phi & 0 \\ 0 & 0 & 1 \end{bmatrix},$$

where Θ and Φ are the desired elevation and azimuth angles of rotation for the radiation pattern states of the RPRAs elements, as illustrated in Fig. 3. The tilt angle relative to the plane of the array, α , as shown in Fig. 1, corresponds to a rotation in elevation of $\Theta = \pi/2 \pm \alpha$, where $-\alpha$ corresponds to the uptilt state and $+\alpha$ corresponds to the downtilt state. The azimuth angle of rotation is based on the position of each element in the UCA, $\Phi = 2(n-1)\pi/N$, since the patterns are directed outward from the center of the array. Thus, the rotated Cartesian representation of the new gain pattern is given by:

$$\begin{bmatrix} G_{nx} \\ G_{ny} \\ G_{nz} \end{bmatrix} = \mathbf{R}_z\left(\frac{2(n-1)\pi}{N}\right) \mathbf{R}_y\left(\frac{\pi}{2} \pm \alpha\right) \begin{bmatrix} \hat{G}_x \\ \hat{G}_y \\ \hat{G}_z \end{bmatrix}, \tag{12}$$

$n = 1 \dots N$,

which can be converted back to spherical coordinates for each RPRAs element, $(G_{nx}, G_{ny}, G_{nz}) \rightarrow G_n(\theta, \phi)$. The resulting patterns can be used in the ARV given by (4) with $g_n^{u/d}(\theta, \phi) = (G_n^{u/d}(\theta, \phi))^{1/2}$. The effect of the exponent, ρ , in (10) on the directivity, D , of the pattern is illustrated in Fig. 4 in the elevation plane for $\alpha = 45^\circ$. For $\rho = 1$, the corresponding directivity of each element state is $D = 3$ dBi, and as ρ increases it can be seen that the pattern becomes more directional with a directivity of approximately $D = 12$ dBi for $\rho = 15$. This form for the theoretical radiation patterns was used to systematically control the

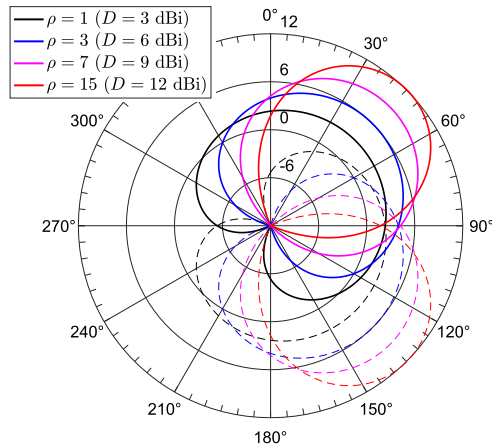


FIGURE 4. Theoretical RPR element elevation plane directivity patterns in dBi for a tilt angle of $\alpha = 45^\circ$ relative to the plane of the UCA (see Fig. 1 for a 3D illustration) for various values of the exponent ρ in (10). Solid lines show the uptilt state and dashed lines show the downtilt state.

directivity and tilt angle to determine the optimal combination that achieves the lowest DoA estimation error, which can then be used as a target for a practical RPR design. It is important to note that the *a priori* selection of the cardioid family of radiation patterns does not necessarily represent a global optimum so future work in this area is of interest to determine if alternate pattern shapes can improve performance while also being realizable as a practical antenna design. However, the previously demonstrated ability to achieve practical antennas that approximate the cardioid pattern make it a reasonable starting point for investigation.

IV. DOA ESTIMATION WITH THEORETICAL RPRAS

In this section, the RPR configurations that provide the most accurate overall 2D DoA estimation are identified for UCAs consisting of $N = 3, 4,$ and 5 elements. The focus is on low numbers of elements since the proposed use of RPRs in UCAs is most attractive for SWaP-constrained platforms that need to minimize receiver channels such as small UAVs and small satellites (for unconstrained platforms, more fixed elements could simply be used rather than the added design complexity of RPRs). The performance of UCAs composed of various numbers of optimized-cardioid theoretical RPRs are compared to each other, as well as to baseline theoretical arrays consisting of non-reconfigurable isotropic antenna elements.

A. CRAMÉR-RAO LOWER BOUND

The Cramér-Rao Lower Bound (CRLB) is a commonly used metric to determine the theoretical limit of estimation accuracy with an unbiased estimator. It is defined as the bound on the covariance matrix of any unbiased parameter estimate and can be determined from the inverse of the Fisher Information Matrix (FIM). Specifically, $\mathbf{C}(\Psi) = \mathbf{F}^{-1}$, where $\mathbf{C}(\Psi)$ is the CRLB of parameter vector Ψ , and \mathbf{F} is the FIM. In the case of 2D DOA estimation, the incident signal angles θ and ϕ are the parameters of interest, but there are also additional unknowns such as the incident signal amplitude,

γ , and phase, δ . Although the incident signal amplitude and phase are not of interest, they are unknowns so they are considered in the CRLB derivation. This results in a multi-parameter estimate for $\Psi = [\theta, \phi, \gamma, \delta]$. With a received signal vector given by \mathbf{x} , the array correlation matrix is given by $\mathbf{R}_{xx} = E[\mathbf{x} \cdot \mathbf{x}^H]$. From [38], the elements of the FIM can be found with

$$\mathbf{F}_{vw} = K \cdot \text{tr} \left[\mathbf{R}_{xx}^{-1} \frac{\partial \mathbf{R}_{xx}}{\partial \Psi_v} \mathbf{R}_{xx}^{-1} \frac{\partial \mathbf{R}_{xx}}{\partial \Psi_w} \right], \quad v, w = 1 \dots 4, \quad (13)$$

where $\text{tr}[\cdot]$ represents the trace operation, and v, w are the indices of the FIM based on the combinations of the parameters in Ψ . The resulting FIM can be partitioned into wanted and unwanted parameters,

$$\mathbf{F} = \begin{bmatrix} F_{\theta\theta} & F_{\theta\phi} & F_{\theta\gamma} & F_{\theta\delta} \\ F_{\phi\theta} & F_{\phi\phi} & F_{\phi\gamma} & F_{\phi\delta} \\ F_{\gamma\theta} & F_{\gamma\phi} & F_{\gamma\gamma} & F_{\gamma\delta} \\ F_{\delta\theta} & F_{\delta\phi} & F_{\delta\gamma} & F_{\delta\delta} \end{bmatrix} = \begin{bmatrix} \mathbf{F}_{(\theta,\phi)(\theta,\phi)} & \mathbf{F}_{(\theta,\phi)(\gamma,\delta)} \\ \mathbf{F}_{(\gamma,\delta)(\theta,\phi)} & \mathbf{F}_{(\gamma,\delta)(\gamma,\delta)} \end{bmatrix} \quad (14)$$

from which the CRLB can be determined:

$$\begin{aligned} \mathbf{C}(\theta, \phi) &= \begin{bmatrix} C_{\theta\theta} & C_{\theta\phi} \\ C_{\phi\theta} & C_{\phi\phi} \end{bmatrix} \\ &= [\mathbf{F}_{(\theta,\phi)(\theta,\phi)} - \mathbf{F}_{(\theta,\phi)(\gamma,\delta)} \mathbf{F}_{(\gamma,\delta)(\gamma,\delta)}^{-1} \mathbf{F}_{(\gamma,\delta)(\theta,\phi)}]^{-1}. \end{aligned} \quad (15)$$

It will later be observed that the $C_{\theta\theta}$ component of the CRLB can be used to optimize the RPRs in UCAs for electrically small array radii.

The CRLB provides local bounds, but does not include the effects of potentially large errors due to ambiguities. Ambiguities can be caused by multiple incident signal angles having identical array response vectors (a type I ambiguity from [34]). A benefit to using directional antennas in UCAs is the ability to use antenna gain information to resolve ambiguities, enabling the use of electrically large array radii [12], as well as potentially enabling ambiguity-free 2D DoA estimation over all incident angles. In order to determine the optimal antenna radiation patterns for 2D DOA estimation in UCAs, the CRLB alone is not sufficient in general, since ambiguities can be a significant potential source of error. There have been a number of formulations of ambiguity functions presented in the literature to characterize this effect (e.g., [39], [40]). Since the MUSIC algorithm approaches the CRLB for uncorrelated signals with high SNR or large numbers of samples, and it also includes the effect of ambiguities, it will be the primary method used to characterize DoA estimation performance. However, the CRLB will first be compared to MUSIC for the case of electrically small array radii where ambiguities are less predominant.

B. RPR OPTIMIZATION

Using the theoretical cardioid radiation pattern family discussed in the previous section, several configurations were

considered and analyzed for their DoA accuracy over all potential azimuth and elevation incident angles, starting with $N = 4$ UCA RPRA elements. The focus will be on low numbers of elements ($N = 3, 4, 5$) since the goal of this work is to achieve unambiguous DoA estimation over all 3D space with a minimal number of independent receiver channels.

For clarity and simplicity, one incident signal is considered at a time. For the MUSIC simulations in this paper, there was a 1° resolution in the DoA search space over all possible 2D angles of arrival, ($\theta = 0^\circ \dots 180^\circ, \phi = 0^\circ \dots 360^\circ$) and 100 trials were run at each incident angle. An incident signal was simulated from each potential azimuth and elevation angle (one at a time), also at a resolution of 1° , and the DoA estimate was computed along with the error using knowledge of the true incident angle. The SNR was initially set to 10 dB and $K = 50$ samples were taken of the incident signal in each of the two RPRA pattern states (i.e., 100 samples in total for each element). For MUSIC, $T = 100$ trials were run at each incident angle and the root mean square error (RMSE) was computed. If the actual incident angle for a particular trial, t , is (θ, ϕ) , and the MUSIC-estimated DoA for that trial is represented by $(\hat{\theta}, \hat{\phi})$, then the angular error, $\epsilon_t(\theta, \phi)$, can be determined by using the dot product to calculate the angle between two vectors pointing from the origin to the surface of the unit sphere. Specifically,

$$\epsilon_t(\theta, \phi) = \cos^{-1}(\cos \theta \cos \hat{\theta} + \sin \theta \sin \hat{\theta} \cos(\phi - \hat{\phi})). \tag{16}$$

which takes into account the impact of elevation angle on azimuth estimates (e.g., an incident signal from $\theta = 0^\circ$ with an estimated $\hat{\theta} = 0^\circ$ should have $\epsilon_t = 0$ regardless of the azimuth estimate $\hat{\phi}$).

Assuming that there is no *a priori* knowledge of potential transmitter locations or of the relative UCA position/orientation, the DoA error associated with each potential incident angle over the full sphere can be weighted equally. In this case, the estimation results for all incident angles can be combined to give an overall error estimate (i.e., a single overall RMSE or CRLB variance for incident signals from $\theta = 0^\circ \dots 180^\circ, \phi = 0^\circ \dots 360^\circ$). By including the performance across all incident angles, the overall error can be used to characterize a particular RPRA element configuration, allowing the optimal tilt angle and directivity to be determined for a specific UCA geometry.

The RMSE was calculated across all possible incident angles ($0^\circ \leq \theta \leq 180^\circ, 0^\circ \leq \phi < 360^\circ$) with a 1° step size using

$$\text{RMSE} = \sqrt{\frac{\sum_{t=1}^T \epsilon_t(\theta, \phi)^2}{T}} \tag{17}$$

for $T = 100$ trials. Shown in Fig. 5 are the CRLB results for various α - D (pattern tilt angle and directivity) RPRA element configurations for an electrically small array with $N = 4, r = \lambda/4$. Fig. 5(a) shows the square root of the $C_{\theta\theta}$ CRLB component (i.e., the standard deviation) from (15), and

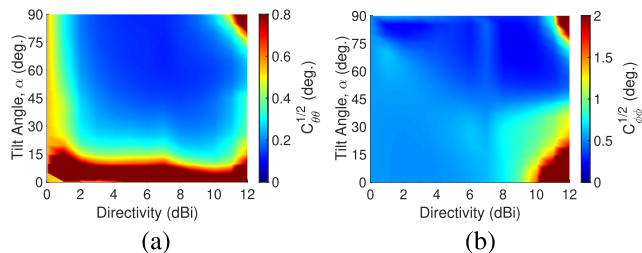


FIGURE 5. Square roots of (a) $C_{\theta\theta}$ and (b) $C_{\phi\phi}$ CRLB components from (15) for a UCA composed of $N = 4$ RPRA elements with radius $r = \lambda/4$ (SNR = 10 dB).

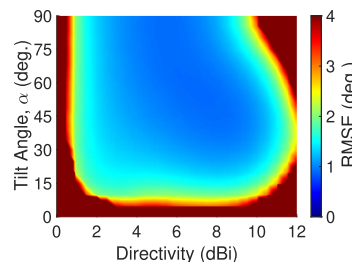


FIGURE 6. RMSE using the MUSIC algorithm for a UCA composed of $N = 4$ RPRA elements with radius $r = \lambda/4$ (SNR = 10 dB).

Fig. 5(b) shows the square root of $C_{\phi\phi}$. Blue areas indicate α - D combinations that result in low overall errors whereas red indicates large errors. For comparison, Fig. 6 shows the MUSIC overall RMSE from (17), which is qualitatively similar to $\sqrt{C_{\theta\theta}}$ in Fig. 5(a). Except for high directivities, the $C_{\phi\phi}$ component of the CRLB is relatively uniform across the α - D domain, which results in the $C_{\theta\theta}$ component being more informative for optimization. The overall error minimum for the RMSE in Fig. 6 is at $\alpha = 55^\circ$ and $D = 7$ dBi, which is similar to the CRLB $\sqrt{C_{\theta\theta}}$ minimum in Fig. 5(a) at $\alpha = 65^\circ$ and $D = 7$ dBi. The results in Fig. 5 and Fig. 6 indicate a relatively wide range of directivities from approximately 3 dBi to 9 dBi at tilt angles from 30° to 90° where the error is close to a minimum. It will later be shown that for larger array radii there is a much narrower range of α - D where the error is minimized. The results also show that relatively low error can be obtained even if the antennas have tilt angles of $\alpha = 90^\circ$ (i.e., pointing directly up and down). As will be discussed in the subsequent results, this is not necessarily the case for larger array radii due to possible ambiguities from incident signals in the plane of the array.

As discussed previously, the use of directive antenna elements can potentially enable the use of larger array radii since the gain variation can be used to resolve phase ambiguities. Furthermore, larger array radii can potentially improve performance, reduce mutual coupling, and increase bandwidth. However, electrically large array radii are accompanied by a potential increase in the effect of ambiguities, which limits the usefulness of the CRLB for pattern optimization. To gain more insight into the performance at various incident angles, an array radii of $r = \lambda$ was used and the RMSE

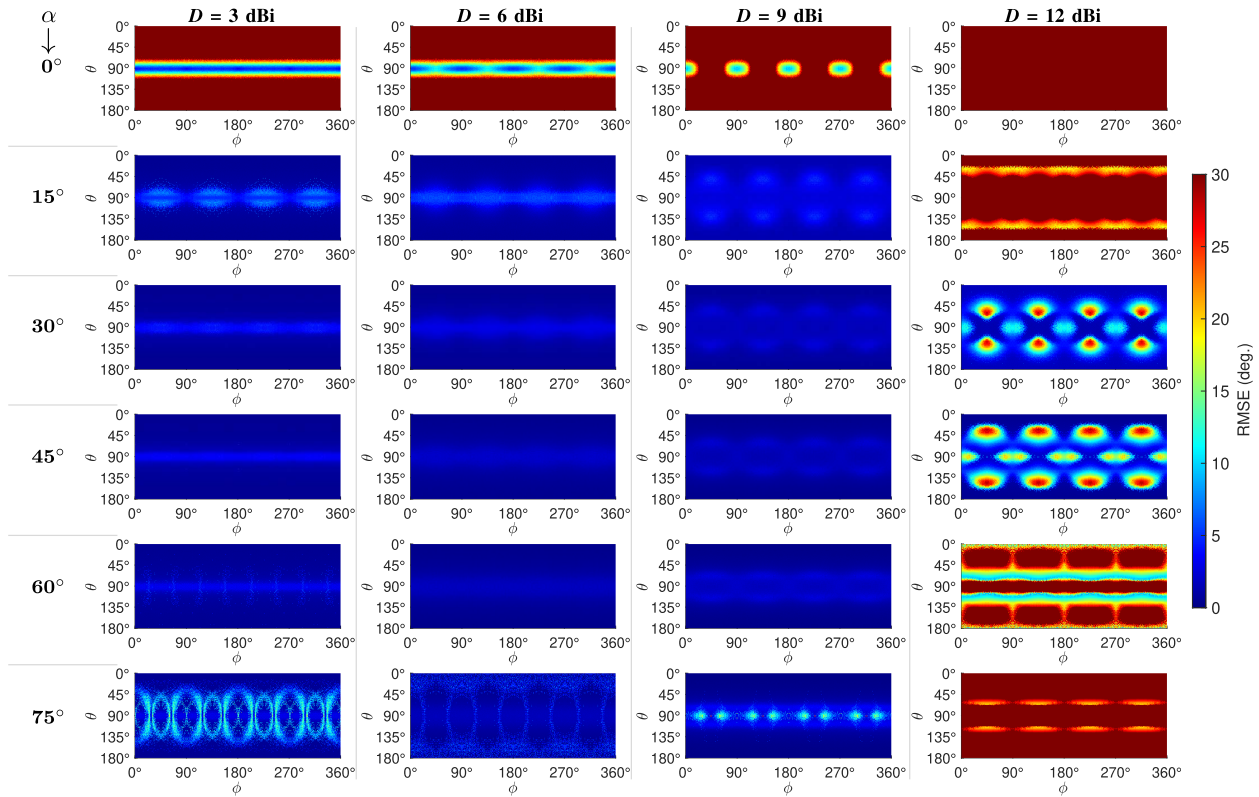


FIGURE 7. DoA estimation accuracy for signals arriving from each potential incident direction (1° resolution, SNR = 0 dB) for various RPRAs tilt angles, α , and directivities, D . The UCA has $r = \lambda$ and is composed of $N = 4$ RPRA elements with two pattern states each (see Fig. 1 for a 3D illustration). The color of each pixel represents the root mean square error for that particular (θ, ϕ) incident angle over $T = 100$ trials.

was determined at each incident angle for several RPRA configurations. Specifically, RPRA tilt angles of $\alpha = 0^\circ, 15^\circ, 30^\circ, 45^\circ, 60^\circ, 75^\circ$ were considered, together with directivities of $D = 3, 6, 9,$ and 12 dBi for an SNR of 0 dB. The results are shown in Fig. 7, where each row represents a particular tilt angle, α , and each column represents a particular element state directivity, D . Whereas Fig. 6 combined the results across all incident angles, Fig. 7 illustrates the error at specific incident angles.

It can be seen from Fig. 7 that for small tilt angles, including no tilt at $\alpha = 0^\circ$ (which is equivalent to a UCA of $N = 4$ non-reconfigurable elements with $2K = 100$ samples) that accurate DoA estimates can only be obtained over a very limited range of incident angles. With $\alpha = 0^\circ$, directive antennas can provide unambiguous DoA estimates in the plane of the array (e.g., see $\alpha = 0^\circ, D = 3$ dBi at $\theta = 90^\circ$ in Fig. 7); however, there is an inherent estimation ambiguity from incident signals at elevation angles above or below the plane of the array. It can also be seen in Fig. 7 that if the directivity is too high then accurate DoA estimates are not possible over all potential incident angles regardless of tilt angle. Qualitatively, from this figure there appears to be a particular range of α - D combinations that result in the lowest estimation errors over all possible incident angles. In particular, a directivity in the range of $D = 6 - 9$ dBi

with $\alpha = 30^\circ - 60^\circ$ appears to give the best performance and do not indicate any large errors due to ambiguities.

To investigate further, the results over all incident angles and across all trials were combined into one total RMSE for each particular α - D combination, similar to Figs. 5 and 6. Shown in Fig. 8 are heatmaps of various α - D combinations for $N = 3, N = 4,$ and $N = 5$ elements for SNRs of -4 dB, -6 dB, and -8 dB, respectively, for array radii $r = \lambda$. From the results in this figure, the tilt-directivity dependence on DoA accuracy is clear, and the combination that minimizes overall estimation error can be quantitatively determined. Specifically, the lowest overall RMSE for $N = 3$ elements occurs at $\alpha = 40^\circ, D = 7$ dBi; for $N = 4$ elements it occurs at $\alpha = 40^\circ, D = 8$ dBi; and for $N = 5$ elements the lowest RMSE also occurs at $\alpha = 40^\circ, D = 8$ dBi. Primarily due to the increased effect of ambiguities at lower SNRs, the optimal element pattern depends on the specific value of SNR used for the analysis. In particular, the ideal tilt angle increases with SNR (e.g., at 10 dB SNR, the optimal pattern for $N = 4, r = \lambda$ occurs for $\alpha = 75^\circ, D = 6$ dBi). In addition, at higher SNRs, lower directivities can still produce relatively accurate estimates (e.g., compare Fig. 7 with Fig. 8(b) for $D = 3$ dBi). One approach to selecting the SNR level for optimization would be to base it on the minimum level of accuracy required for the application of interest. Once

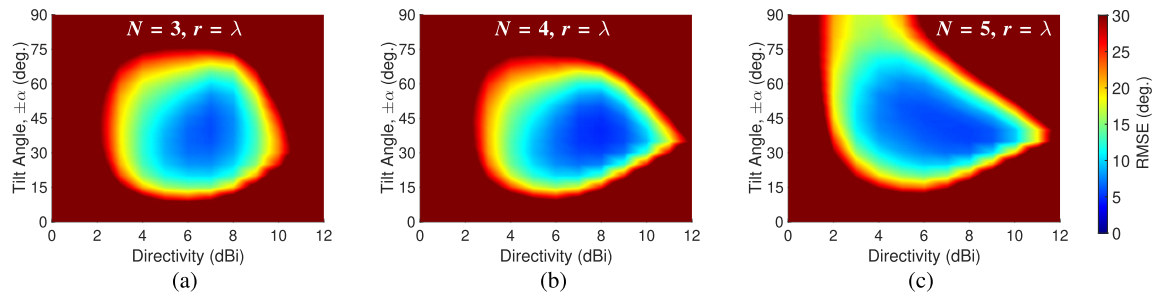


FIGURE 8. Overall RMSE of DoA estimation across all incident angles showing the performance at various combinations of elevation tilt angles, α , and directivities, D , for UCAs that have (a) $N = 3$ RPRA elements spaced at $r = \lambda$ (SNR = -4 dB), (b) $N = 4$ RPRA elements spaced at $r = \lambda$ (SNR = -6 dB), and (c) $N = 5$ RPRA elements spaced at $r = \lambda$ (SNR = -8 dB).

this is determined, the lowest SNR that can achieve this accuracy can be used for optimization in order to provide the greatest operational range of SNRs. For some applications, extremely accurate ($< 1^\circ$) DoA estimation may be required, whereas for other applications such as electronic warfare, for example, the threshold may be somewhat higher. For this work, as an example, the minimum accuracy is assumed to be 5° RMSE, which corresponds to the SNR levels used in Fig. 8.

Comparing Fig. 8(a) and (b), it can be seen that the optimal directivity has increased along with the increased number of elements, which makes intuitive sense since each antenna in the $N = 4$ UCA has a smaller spatial area to cover compared to the $N = 3$ case. However, Fig. 8(c) shows a significantly different dependence on α and D . For example, it can be seen that for $N = 5$, tilt angles as high as $\alpha = 90^\circ$ (patterns pointed directly up and down, perpendicular to the plane of the array) can still provide somewhat accurate DoA estimates around $D = 4$ dBi in contrast with the results for $N = 3$ and $N = 4$ in Fig. 8(a) and (b). This is somewhat similar to the $r = \lambda/4$ case in Fig. 6 where relatively accurate estimations were possible up to $\alpha = 90^\circ$. As $\alpha \rightarrow 90^\circ$ the radiation pattern for the uptilt state approaches the $\hat{G}(\theta, \phi)$ pattern in Fig. 3, and for the downtilt state it is directed toward the $-z$ -axis. As a consequence, the patterns in the plane of the array become increasingly omnidirectional. As such, the DoA estimation performance in the plane of the array approaches that of a UCA composed of omnidirectional elements, which is limited in its ability to provide unambiguous DoA estimates in the array plane based on the number of elements and the array radius. Specifically, for a UCA with $N = 4$ omnidirectional elements, unambiguous DoA estimates can only be obtained in the plane of the array for $r < \lambda/(2\sqrt{2})$ because beyond this radius there are multiple incident angles that produce identical element excitations. Since Fig. 8 is for $r = \lambda$, the $N = 3$ and $N = 4$ cases produce ambiguous estimates as $\alpha \rightarrow 90^\circ$ because the patterns become omnidirectional in the plane of the UCA. In contrast, for the $N = 5$ case, a UCA with $r = \lambda$ is able to provide unambiguous DoA estimates with omnidirectional elements in the plane of the array. Clearly, however, this is not the ideal configuration, and better performance can be obtained by using tilt angles in the approximate range of 30°

to 50° , similar to the $N = 3$ and $N = 4$ cases. Furthermore, it can be observed from Fig. 8 that for all three cases the configuration of $\alpha \approx 40^\circ$ provides the widest range of directivities over which accurate DoA can be achieved, which in turn can increase the tolerance for a practical antenna design. The remainder of the results will focus specifically on the tilt angle and directivity combinations that provide the best performance. Each configuration in Fig. 8 produces the most accurate DoA with $\alpha = 40^\circ$, so this tilt angle will be used together with the optimal directivities for $N = 3$ (7 dBi), $N = 4$ (8 dBi), and $N = 5$ (8 dBi).

The effect of various array radii for the $N = 4$ configuration is shown in Fig. 9 as the SNR increases from -20 dB to 10 dB for the optimal cardioid pattern based on the results in Fig. 8(b) ($\alpha = 40^\circ, D = 8$ dBi). From this figure it is clear that the performance is not strongly dependent on the array radius. This is a very attractive feature since similar DoA estimation performance can be realized for a variety of different physical installation platforms over an extremely wide range of frequencies without requiring a different antenna element design. From the inset of Fig. 9, it is clear that a larger array radii can achieve lower RMSE at high SNRs, and that accurate DoA estimates are possible over at least a two decade bandwidth. Practically speaking, the bandwidth would be limited by the RPRA elements and not the array geometry.

While the DoA estimation performance is not highly sensitive to array radius for the particular directivity shown in Fig. 9 (8 dBi), this is not necessarily the case for other element directivities. The effect of directivity on RMSE for seven different array radii is shown in Fig. 10 with $N = 4, \alpha = 40^\circ$, and an SNR of -6 dB. From this figure it can be seen that a directivity of $D = 8$ dBi corresponds to the minimum for the $r = \lambda$ case, as expected from previous results, and is also a reasonable compromise value for array radii spanning from $r = \lambda/10$ to $r = 10\lambda$. However, alternative values of directivity can result in somewhat lower RMSEs if the design is to be optimized for a particular array radius. Fig. 10 shows that as the array radius increases, the optimal directivity approaches $D \approx 8.5$ dBi. Note that all configurations have a rapidly increasing RMSE for low directivities. As the directivity is reduced, there is less pattern variation for different incident directions (particularly in

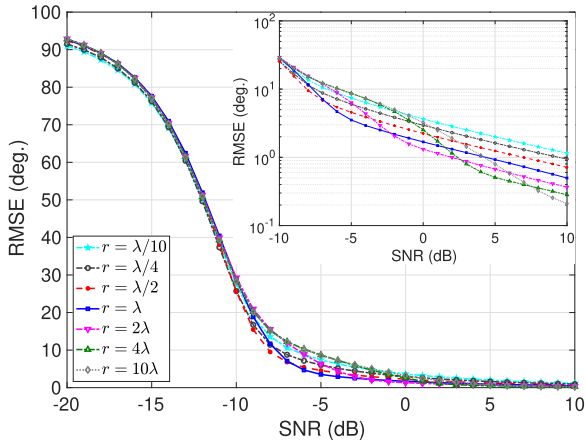


FIGURE 9. DoA estimation RMSE for a UCA consisting of $N = 4$ RPRA elements ($D = 8$ dBi, $\alpha = 40^\circ$) with various array radii to show the effect of array dimensions and/or signal frequency on estimation accuracy. *Inset:* Logarithmic scale to more clearly distinguish performance at high SNRs.

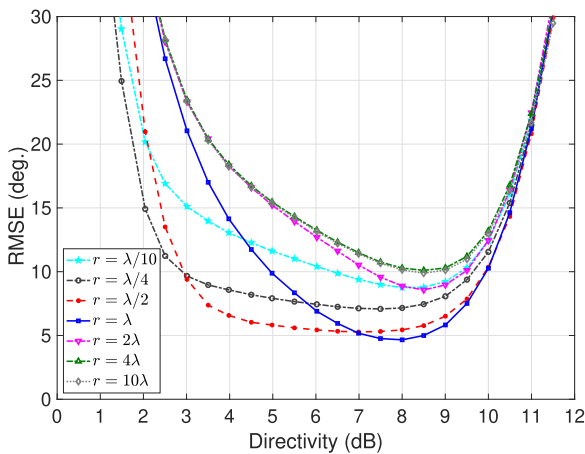


FIGURE 10. DoA estimation RMSE for a UCA consisting of $N = 4$ RPRA elements ($\alpha = 40^\circ$) with varying directivities for several different UCA radii (SNR = -6 dB).

elevation), which leads to an increase in ambiguous estimates and large errors.

While the optimization results presented in this section were determined specifically for the cardioid family of radiation patterns, it is expected that the results would be similar for alternative theoretical unidirectional pattern types. Non-unidirectional theoretical RPRA patterns could possibly provide performance advantages and these could be explored by following an approach similar to the one presented here. A parasitic patch RPRA design is presented in Section V that demonstrates DoA performance very similar to the cardioid theoretical results even with the inevitable pattern discrepancies that occur when implementing a practical antenna design. This similarity in performance despite pattern differences indicates that the optimization results are not highly dependent on achieving a precise cardioid pattern.

C. PERFORMANCE COMPARISONS

The results from the previous section showed that it is possible to obtain unambiguous DoA estimation over all

possible 2D incident angles with UCAs by using RPRA elements that have optimized cardioid patterns. A natural question follows regarding the performance of such RPRA UCAs composed of different numbers of elements, as well as the performance compared to conventional arrays with fixed antenna elements. In order to make comparisons, the conventional array geometries and fixed element patterns must be selected, as well as the specific RPRA UCA configurations. Since incident angles from all potential directions ($\theta = 0^\circ \dots 180^\circ$, $\phi = 0^\circ \dots 360^\circ$) are of interest, reference arrays with 3D array geometries, such as uniform cylindrical arrays and uniform spherical arrays, are most suitable to minimize the effect of ambiguities. Since uniform cylindrical arrays are composed of multiple concentric UCAs that are offset vertically, and spherical arrays have array elements dispersed around the surface of a sphere, the (x, y, z) variation of the element positions can potentially provide the response diversity needed for unambiguous 2D DoA estimation.

For the elements in the conventional fixed arrays, rather than arbitrarily select a pattern with a particular directivity, theoretical isotropic antennas will be used for generality in order to make baseline comparisons with the UCAs composed of RPRAs. Specifically, three configurations of arrays composed of non-reconfigurable isotropic elements were considered: (i) a 6-element uniform spherical array (*Fixed USpha-6*) with radius r , which is equivalent to elements positioned on each side of a cube; (ii) an 8-element uniform spherical array (*Fixed USpha-8*) equivalent to elements positioned at the corners of a cube that is inscribed by a sphere with radius r ; (iii) an 8-element uniform cylindrical array (*Fixed UCylA-8*) consisting of two vertically offset 4-element UCA subarrays with radius r .

With isotropic elements, both the UCylA and USpha will have ambiguities if the array radii are too large. For example, the onset of ambiguities for the *Fixed UCylA-8* occurs at $r = \lambda/(2\sqrt{2})$ (for incident signals at $\theta = 90^\circ$ for $\phi = 45^\circ, 135^\circ, 225^\circ, 315^\circ$) and for the *Fixed USpha-6* ambiguities occur at $r = \lambda/2$ (for incident signals at $\theta = 0^\circ, 180^\circ$, and $\theta = 90^\circ$ for $\phi = 0^\circ, 90^\circ, 180^\circ, 270^\circ$). The RPRA UCA will greatly outperform the conventional baseline arrays for electrical large radii due to these ambiguities, and therefore, an electrically small array radii of $r = \lambda/4$ will be used for a comparison with the theoretical baseline arrays.

For the *Fixed UCylA-8*, the vertical separation of the elements is also set equal to $\lambda/4$ for uniformity and to be significantly away from the spacing that would produce ambiguities due to signals arriving from $\theta = 0^\circ, 180^\circ$ (which would occur at a separation of $\lambda/2$). Of course, uniform cylindrical arrays could be implemented with directive elements that have elevation tilt angles, similar to the RPRAs. For that case, the results in this paper regarding optimal tilt angle and directivity are informative for the non-reconfigurable elements since, to the best of the author's knowledge, this information has not been previously presented in the literature. However, this approach of using

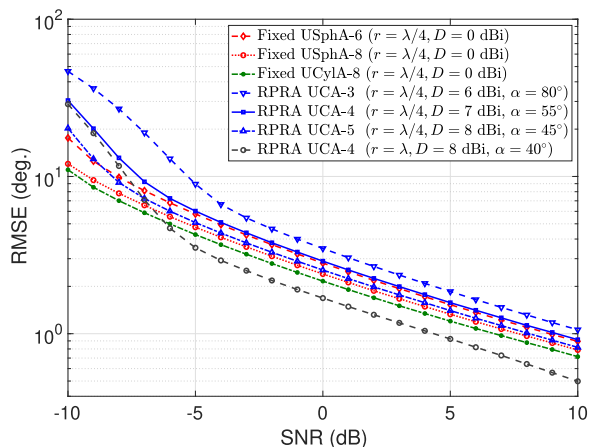


FIGURE 11. DoA estimation performance of theoretical arrays that use isotropic elements in comparison to UCAs that consist of $N = 3, 4,$ and 5 optimized-cardioid RPR elements.

non-reconfigurable UCylA elements with elevation pattern variation would come at the expense of an increased number of RF front-ends/ADCs, the minimization of which is a primary purpose of the proposed technique using RPRAs.

In order to fairly compare the performance of arrays using fixed elements with UCAs using reconfigurable elements, the total sampling period and the total number of samples per element should be equal. For the RPR element, samples are taken in each of the two states, whereas fixed elements can receive twice the number of samples for the same sampling period. Specifically, for the comparisons in this section, $K = 50$ samples are used for each state of the RPRAs, whereas $2K = 100$ samples are used for each non-reconfigurable element in order to estimate the DoA.

Using the results from Fig. 6 for $N = 4, r = \lambda/4$ along with similar results for $N = 3$ and $N = 5$ (not shown), the optimum RPR configurations are compared with the three baseline theoretical arrays composed of isotropic elements as discussed above. The optimal cardioid RPR patterns for $r = \lambda/4$ UCAs are: (i) *RPR A UCA-3*: $N = 3, \alpha = 80^\circ, D = 6$ dBi, (ii) *RPR A UCA-4*: $N = 4, \alpha = 55^\circ, D = 7$ dBi, and (iii) *RPR A UCA-5*: $N = 5, \alpha = 45^\circ, D = 8$ dBi.

The overall RMSEs across all incident angles (1° step size) with $T = 100$ trials at each angle are shown in Fig. 11 as the SNR is swept for the various array configurations. From this figure, it is clear that the performance of *RPR A UCA-4* is almost identical to *Fixed USphA-6* once the SNR is above -5 dB. Specifically, in terms of SNR, the performance of *RPR A UCA-4* is degraded by only 0.25 dB compared to *Fixed USphA-6*, while requiring only four receiver channels. Compared to the *Fixed USphA-8*, the *RPR A UCA-5* performance is reduced by 0.5 dB in terms of SNR and by approximately 1 dB compared to *Fixed UCylA-8*. For reference, also shown in Fig. 11 is the *RPR A UCA-4* with a larger array radii ($r = \lambda$) which was optimized using Fig. 8(b) (*RPR A UCA-4*: $N = 4, \alpha = 40^\circ, D = 8$ dBi). The electrically larger array radii demonstrates significantly

improved accuracy in addition to other possible benefits such as reduced mutual coupling. Fig. 11 demonstrates that the added diversity in radiation patterns through the use of RPRAs can largely overcome the reduced number of samples captured in each state compared to theoretical baseline arrays with more elements.

The RPRAs considered in this work were limited to two states for simplicity. It may be advantageous to use more pattern states; however, for a fixed sampling period there is a tradeoff between the number of states and the number of samples that can be obtained in each state.

Direct quantitative comparisons with other DoA estimation approaches using RPRAs are difficult since the prior work in [16]–[33] has focused on individual RPRAs with mode selection/switching and/or does not include comprehensive 2D DoA estimation performance over all possible incident angles. Compared to [21]–[26], the proposed approach using two-state RPRAs in a UCA would generally require less total sampling time and should achieve higher accuracy since the CRLH LWAs have a limited number of states (though that approach can perform DoA estimation with a single front-end). Only 1D DoA estimation was shown in those works, however, the CRLH LWA designs presented could potentially be used as the RPR elements in a UCA for 2D DoA estimation.

To summarize, assuming practical RPR elements can be designed to approximate the radiation patterns presented in this section, the potential advantages of the proposed approach include:

- (i) Unambiguous 2D DoA estimation over the full range of potential incident angles ($\theta = 0^\circ \dots 180^\circ, \phi = 0^\circ \dots 360^\circ$).
- (ii) Minimal numbers of independent receiver channels required (e.g., see Fig. 11 compared to the USphA-6).
- (iii) Wide bandwidth, limited only by the RPR element bandwidth, and not the array radius (e.g., see Fig. 9).
- (iv) Ability to use electrically large or small array radii with a single optimized RPR design (e.g. see Fig. 10).
- (v) Orientation-independent UCA geometry (i.e., the elements can be positioned in any 2D plane) with no center element required.

V. PRACTICAL RPR DESIGN AND DoA PERFORMANCE

The analysis and results presented thus far have been based entirely on theoretical radiation patterns with the basic shape defined by (10) and have not considered practical antenna design aspects. In order to realize the advantages of the proposed technique and demonstrate its practicality, an RPR would need to be designed that has radiation pattern states that approximate the optimal theoretical cardioid pattern determined in Section IV. This section presents an example of such a design using the optimal result found for the 4- and 5-element UCAs with radii of $r = \lambda$. A C-band frequency of 6 GHz was selected for the design with a corresponding array radius of $r = 5$ cm. This particular radius corresponds to the scenario of having an

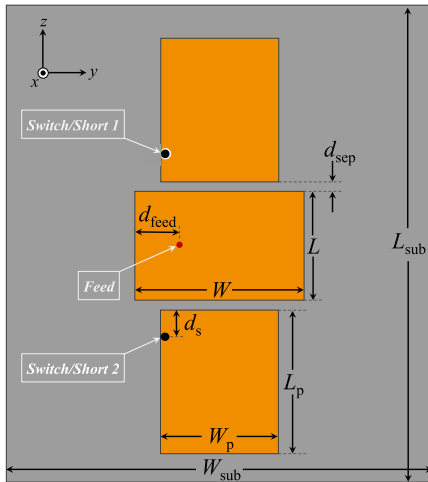


FIGURE 12. Diagram of the RPR using two parasitic patches with a switch on each to control the electrical connection to shorting vias that go to the ground plane underneath. A small gap is illustrated around *Switch/Short 1* representing an open switch state while *Switch/Short 2* is closed. This switch configuration corresponds to the uptilt pattern state (see Figs. 1, 13, and 14).

RPR on four sides of a CubeSat (e.g., a 1U, 2U, or 3U) for $N = 4$, though for simplicity and generality, the electromagnetic (EM) simulations do not include a model of the platform. For optimal performance for a particular application, the mounting platform could be included as part of the antenna design and optimization process.

The best performance for the $N = 4$ and $N = 5$ UCAs with $r = \lambda$ was found to occur with RPRAs having tilt angles of $\alpha = 40^\circ$ and directivities of $D = 8$ dBi. As such, these values served as design goals for the practical RPR example discussed in this section.

A. RPR DESIGN AND SIMULATION

There are a variety of RPRAs that have been presented in the literature that could potentially be suited for the proposed application as the element in a UCA for 2D direction finding, many of which use RF switches to electrically connect or disconnect sections of conductors (e.g., see the RPR designs discussed in [1], [2], [21]–[29], [41]–[43]). For example, in [41] both beam steering and resonant frequency reconfigurability was shown using a grid structure composed of different sized patches along with RF MEMS switches, and it was able to achieve beam tilting over a range of 120° . As another example, in [42], [43], a series of switches was used in parasitic layer-based multifunctional reconfigurable antennas to achieve both radiation pattern and polarization reconfigurability. Depending on the RPR design, it is possible to achieve radiation pattern reconfigurability with a negligible increase in SWaP compared to fixed-beam non-reconfigurable antennas. The proposed practical RPR in this paper is a rectangular patch antenna that uses two parasitic elements and switches as shown in Fig. 12 [44]. Depending on the switch implementation, there could be

TABLE 1. RPR antenna dimensions in units of millimeters.

W_{sub}	L_{sub}	W	L	W_p	L_p	d_{feed}	d_{sep}	d_s
47.9	48.6	17.6	9.3	14.6	19.2	4.8	0.4	2.1

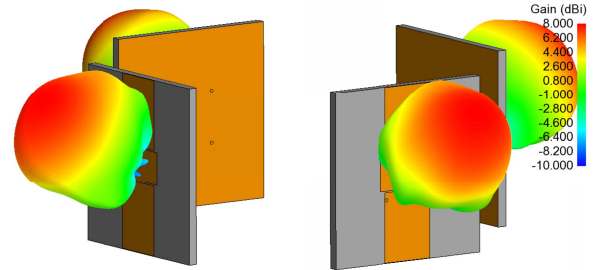


FIGURE 13. 3D radiation pattern of the proposed 6 GHz parasitic patch RPR in the uptilt state for a 4-element UCA with radii $r = \lambda$.

little to no added power consumption with the use of this RPR (e.g., if RF MEMS switches were used). Circular polarization could be beneficial for many applications, but linear polarization will be used here for demonstration, similar to the 2D DoA estimation in [7], [13], [17], [33].

The substrate used for the proposed design is the Rogers Corporation 5880LZ ($\epsilon_r = 2.0$, $\tan \delta = 0.0021$) with a thickness of 2.54 mm. The center patch is probe-fed from behind in the position indicated in Fig. 12 a distance d_{feed} from the edge. The bottom of the substrate serves as the ground plane and is entirely covered in conductor with the exception of a small hole for the feed. The driven patch is centered on the substrate and is separated from the parasitic patches by a distance d_{sep} . Shorting vias/pins that are connected to the ground plane below are positioned on each parasitic patch a distance d_s from the edge closest to the center patch and are located along the side as shown. Switches control the connection of the parasitic patches to the vias, which is what controls the radiation pattern state. To implement the switches in EM simulations, a small gap of 0.5 mm is used for an open switch (see *Switch/Short 1* in Fig. 12) and conductor is used for the closed switch (*Switch/Short 2* in Fig. 12). The design is symmetric about the y -axis and thus has the same pattern shape in the two states. The radiation pattern is tilted in the direction of the open switch (i.e., Fig. 12 is for the uptilt state) with the shorted parasitic patch acting as a reflector and the open-switch parasitic patch serving as a director element.

As mentioned previously, the design goals for the RPR correspond to the optimal configuration found with the theoretical cardioid pattern for $N = 4$ and $N = 5$; namely, a tilt angle of $\alpha = 40^\circ$ and directivity of $D = 8$ dBi with a shape that approximates the mathematical cardioid pattern with $\rho = 5.31$. In addition, the antenna needs to have a suitably low reflection coefficient magnitude and high efficiency so that the overall realized gain is close to the goal directivity. Achieving all of these design goals simultaneously would be laborious and difficult to manually

realize in EM simulations. As such, the design was fully parameterized and a number of optimization techniques were explored including the genetic algorithm, particle swarm optimization, and the Nelder–Mead method using Altair Feko. The desired theoretical radiation pattern found in Section IV was used for the optimization goal function along with a reflection coefficient requirement. More specifically, the goal function was a combination of (i) the primary elevation pattern cut (the xz -plane in Fig. 12), (ii) the azimuth pattern cut at $\theta = 50^\circ$ for the uptilt state since this corresponds to where the gain would be maximum for $\alpha = 40^\circ$, and (iii) $|S_{11}| < -10$ dB. The best results were achieved with the Nelder–Mead method, which produced the RPRAs dimensions shown in Table 1 in units of millimeters. The RPRAs element optimization was performed in isolation without including the effects of mutual coupling between RPRAs elements for computational efficiency. However, once the optimum isolated element was found, it was implemented in an array EM simulation to include the effects of mutual coupling in the DoA estimation results.

The resulting 3D radiation patterns for the uptilt state are shown in Fig. 13 when the RPRAs elements are in an $N = 4$, $r = \lambda$ array. Fig. 14 shows the elevation pattern cut for one of the elements for the RPRAs in isolation and in an $N = 4$, $r = \lambda$ array. It can be seen that the effects of mutual coupling are minor due to the relatively large array radii, and that the cross-polarized response is more than 10 dB below the co-polarized response. Also shown in Fig. 14 are the EM simulation results compared to the desired theoretical cardioid pattern. It is clear that a relatively good match with the theoretical radiation pattern was achieved with the primary differences being a slightly lower tilt angle and more backside radiation (though it is still below -10 dBi). The azimuth pattern (not shown) indicates a similar match to the theoretical goal pattern. The maximum gain of the parasitic patch RPRAs was simulated to be 8.0 dBi at an elevation angle of $\alpha = 34^\circ$. The results from Fig. 8(b) show that a small change in tilt angle around the optimal $\alpha = 40^\circ$ produces similarly low RMSE, so the small reduction in the practical RPRAs tilt angle should not cause a large degradation in estimation accuracy. As mentioned, due to symmetry the downtilt state pattern has the same shape and is mirrored across the xy -plane. The magnitude of the input reflection coefficient is shown in Fig. 15 and has a value of -10.8 dB at 6 GHz, which meets the design goal of $|S_{11}| < -10$ dB.

B. DoA PERFORMANCE WITH PRACTICAL RPRAs ELEMENTS

In order to determine the DoA estimation performance of the parasitic patch RPRAs design, the EM-simulated 3D radiation patterns including the effects of mutual coupling were used for the UCA element patterns in numerical simulations. Consistent with the configuration used to produce Fig. 11, this simulation consisted of incident signals coming from all potential (θ, ϕ) directions with a 1° resolution and $T = 100$ trials at each incident angle. Co-polarized incident

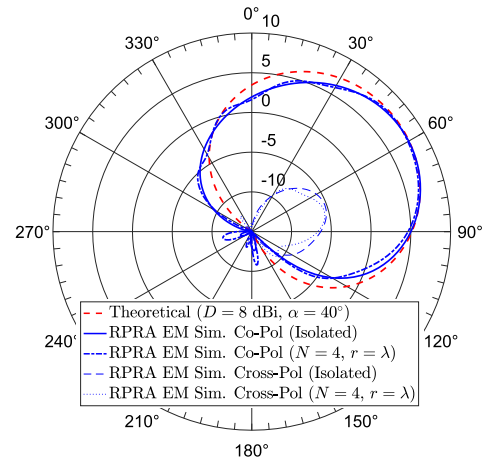


FIGURE 14. Parasitic patch RPRAs gain pattern (elevation plane) compared to the theoretical cardioid elevation pattern with $\alpha = 40^\circ$, $D = 8$ dBi (radial units in dBi).

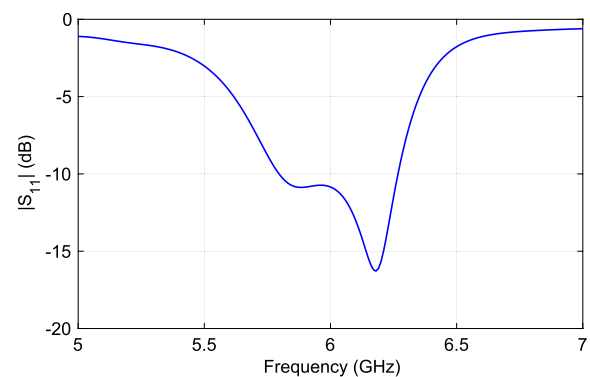


FIGURE 15. Parasitic patch RPRAs input reflection coefficient magnitude.

waves were used for clarity and simplicity as is common in many prior works (e.g., [4], [5], [7], [13], [17], [21]–[26], [29], [33]). The DoA was estimated for each trial, and the overall RMSE across all trials and all incident angles was computed.

The DoA estimation performance for UCAs using parasitic patch RPRAs is presented in Fig. 16 along with the theoretical optimal cardioid results. The 4-element UCA with parasitic patch RPRAs shows very similar performance compared to the theoretical result for SNRs above -4 dB (RMSEs less than 3°). In fact, there is a slight performance improvement at higher SNRs with the practical RPRAs design. Similarly, the results for a 5-element parasitic patch RPRAs UCA are very similar to the theoretical cardioid pattern results for SNRs above -6 dB (RMSEs less than 3°). These results demonstrate that practical RPRAs elements can be realized that achieve DoA performance close to the theoretical results. In Section IV, the optimal cardioid pattern for the 3-element RPRAs UCA had a directivity of 7 dBi as opposed to the 8 dBi in the parasitic patch RPRAs. Though not optimal, the designed parasitic patch RPRAs was applied to a 3-element UCA, and the results are also shown in Fig. 16.

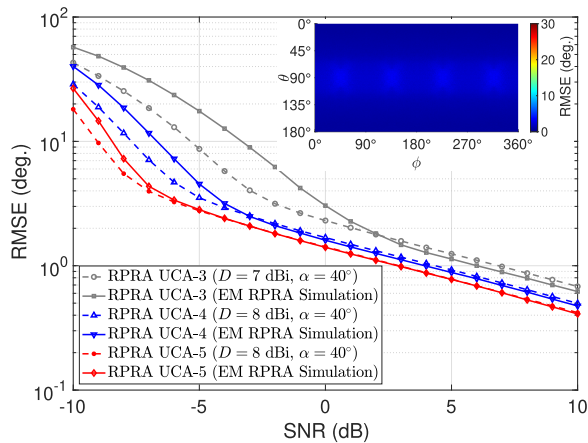


FIGURE 16. DoA estimation accuracy comparison between the proposed parasitic patch RPRAs and the optimal theoretical cardioid patterns for a UCA with radius $r = \lambda$. Inset: RMSE heatmap across all incident angles for the parasitic patch 4-element RPRAs ($r = \lambda$, SNR = 0 dB).

The 3-element RPRAs in Fig. 8(a) was for an SNR of -4 dB to achieve an RMSE less than 5° . As such, the performance of the theoretical cardioid pattern is significantly better than the parasitic patch at this level of SNR. However, while the parasitic patch shows reduced performance at low-SNRs, it exceeds the performance of the theoretical cardioid pattern beyond SNRs of 2 dB. This result illustrates the impact of SNR selection for optimization that was discussed in Section IV.

Also included in Fig. 16 is an inset figure that shows the RMSE heatmap across all azimuth and elevation incident angles for the 4-element UCA using the parasitic patch RPRAs design. This inset figure has a 1° resolution, and each pixel color represents the RMSE over 100 trials from an incident signal impinging on the array from a particular (θ, ϕ) with an SNR of 0 dB (i.e., the same simulation configuration as in Fig. 7). This result shows that accurate and unambiguous 2D DoA estimation over all potential incident angles can be achieved with UCAs using practical optimized RPRAs with relatively few independent receiver channels.

VI. CONCLUSION

The use of radiation pattern reconfigurable antennas for 2D DoA estimation in uniform circular arrays has been systematically studied. Theoretical cardioid-type patterns were used in numerical simulations to determine the optimal radiation pattern states that result in the most accurate DoA estimation over all potential azimuth and elevation incident signal angles. The performance of the optimized RPRAs UCAs was compared to baseline theoretical arrays consisting of isotropic elements, and the results indicated that similar performance could be achieved with fewer antennas/front-ends. A practical parasitic patch RPRAs was designed at 6 GHz to closely approximate the theoretical cardioid pattern states that showed the best performance for 4- and 5-element UCAs. Electromagnetic simulations of the

RPRAs radiation patterns were used to determine the resulting DoA estimation accuracy in comparison to the optimized theoretical cardioid patterns. The results showed that similar performance can be achieved with a simple parasitic patch RPRAs design, thus demonstrating the feasibility of using RPRAs in UCAs to obtain unambiguous 2D DoA estimates. The proposed approach could enable new applications for adaptive arrays since the UCA is orientation-independent, broadband (limited only by RPRAs element bandwidth), and minimal numbers of independent receiver channels are needed which could potentially reduce size, weight, power, and cost.

REFERENCES

- [1] C. G. Christodoulou, Y. Tawk, S. A. Lane, and S. R. Erwin, "Reconfigurable antennas for wireless and space applications," *Proc. IEEE*, vol. 100, no. 7, pp. 2250–2261, Jul. 2012.
- [2] J. Costantine, Y. Tawk, S. E. Barbin, and C. G. Christodoulou, "Reconfigurable antennas: Design and applications," *Proc. IEEE*, vol. 103, no. 3, pp. 424–437, Mar. 2015.
- [3] P. K. Bailleul, "A new era in elemental digital beamforming for spaceborne communications phased arrays," *Proc. IEEE*, vol. 104, no. 3, pp. 623–632, Mar. 2016.
- [4] D. M. Kitavi, K. T. Wong, and C.-C. Hung, "An L-shaped array with nonorthogonal axes—Its Cramér–Rao bound for direction finding," *IEEE Trans. Aerosp. Electron. Syst.*, vol. 54, no. 1, pp. 486–492, Feb. 2018.
- [5] H. Gazzah and S. Marcos, "Analysis and design of (non-)isotropic arrays for 3D direction finding," in *Proc. IEEE/SP 13th Workshop Stat. Signal Process.*, Jul. 2005, pp. 491–496.
- [6] A. Osman, M. M. E. Moussa, M. Tamazin, M. J. Korenberg, and A. Noureldin, "DOA elevation and azimuth angles estimation of GPS jamming signals using fast orthogonal search," *IEEE Trans. Aerosp. Electron. Syst.*, vol. 56, no. 5, pp. 3812–3821, Oct. 2020.
- [7] S. Mohammadi, A. Ghani, and S. H. Sedighy, "Direction-of-arrival estimation in conformal microstrip patch array antenna," *IEEE Trans. Antennas Propag.*, vol. 66, no. 1, pp. 511–515, Jan. 2018.
- [8] H. Gazzah, "Direction finding antenna arrays with improved accuracy and reduced complexity and size," in *Proc. Sensor Signal Process. Defence (SSPD)*, Sep. 2016, pp. 1–5.
- [9] H. Gazzah, "A maneuvering uniform circular array of directional sensors for improved source localization accuracy," *IEEE Trans. Aerosp. Electron. Syst.*, vol. 54, no. 3, pp. 1545–1554, Jun. 2018.
- [10] M. Chen, X. Mao, R. Guo, M. Cao, and Y. Liu, "Design methods for ULA-based directional antenna arrays by shaping the Cramér–Rao bound functions," *IET Signal Process.*, vol. 12, no. 2, pp. 247–254, 2018.
- [11] H. Gazzah and J. P. Delmas, "On isotropic circular arrays of anisotropic sensors," in *Proc. IEEE Int. Symp. Signal Process. Inf. Technol. (ISSPIT)*, Dec. 2015, pp. 95–99.
- [12] B. R. Jackson, S. Rajan, B. J. Liao, and S. Wang, "Direction of arrival estimation using directive antennas in uniform circular arrays," *IEEE Trans. Antennas Propag.*, vol. 63, no. 2, pp. 736–747, Feb. 2015.
- [13] Y. B. Nechaev and I. W. Peshkov, "Evaluation of the influence of directivity factor of directive elements of conformal antenna arrays on the performances of azimuth-elevation DOA estimation," in *Proc. Prog. Electromagn. Res. Symp.-Spring (PIERS)*, 2017, pp. 490–495.
- [14] C. Y. Kataria, G. X. Gao, and J. T. Bernhard, "Design of a compact hemispherical GPS antenna with direction finding capabilities," *IEEE Trans. Antennas Propag.*, vol. 67, no. 5, pp. 2878–2885, May 2019.
- [15] H. Gazzah, "Quasi-isotropic circular arrays of anisotropic sensors," in *Proc. Int. Conf. Electr. Comput. Technol. Appl. (ICECTA)*, Nov. 2017, pp. 1–5.
- [16] A. C. Gurbuz and B. Cetiner, "Multifunctional reconfigurable antennas for cognitive radars," in *Proc. IEEE Radar Conf. (RadarConf)*, Apr. 2018, pp. 1510–1515.
- [17] E. Kaderli, I. Bahceci, K. M. Kaplan, and B. A. Cetiner, "On the use of reconfigurable antenna arrays for DoA estimation of correlated signals," in *Proc. IEEE Radar Conf. (RadarConf)*, May 2016, pp. 1–5.

- [18] J. Tabrikian, O. Isaacs, and I. Bilik, "Cognitive antenna selection for DOA estimation in automotive radar," in *Proc. IEEE Radar Conf. (RadarConf)*, May 2016, pp. 1–5.
- [19] X. Wang, E. Aboutanios, M. Trinkle, and M. G. Amin, "Reconfigurable adaptive array beamforming by antenna selection," *IEEE Trans. Signal Process.*, vol. 62, no. 9, pp. 2385–2396, May 2014.
- [20] K. R. Schab, E. L. Daly, and J. T. Bernhard, "Direction estimation using compressive array sensing and pattern reconfigurable antennas," in *Proc. Asilomar Conf. Signals, Syst. Comput.*, Nov. 2013, pp. 927–930.
- [21] H. Paaso, N. Gulati, D. Patron, A. Hakkarainen, J. Werner, K. R. Dandekar, M. Valkama, and A. Mammela, "DoA estimation using compact CRLH leaky-wave antennas: Novel algorithms and measured performance," *IEEE Trans. Antennas Propag.*, vol. 65, no. 9, pp. 4836–4849, Sep. 2017.
- [22] J. Werner, J. Wang, A. Hakkarainen, D. Cabric, and M. Valkama, "Performance and Cramér–Rao bounds for DoA/RSS estimation and transmitter localization using sectorized antennas," *IEEE Trans. Veh. Technol.*, vol. 65, no. 5, pp. 3255–3270, May 2016.
- [23] A. Hakkarainen, J. Werner, N. Gulati, D. Patron, D. Pfeil, H. Paaso, A. Mammela, K. Dandekar, and M. Valkama, "Reconfigurable antenna based DOA estimation and localization in cognitive radios: Low complexity algorithms and practical measurements," in *Proc. 9th Int. Conf. Cogn. Radio Oriented Wireless Netw. Commun. (CROWNCOM)*, Jun. 2014, pp. 454–459.
- [24] V. Vakilian, J.-F. Frigon, and S. Roy, "Effects of angle-of-arrival estimation errors, angular spread and antenna beamwidth on the performance of reconfigurable SISO systems," in *Proc. IEEE Pacific Rim Conf. Commun., Comput. Signal Process.*, Aug. 2011, pp. 515–519.
- [25] V. Vakilian, H. V. Nguyen, S. Abielmona, S. Roy, and J.-F. Frigon, "Experimental study of direction-of-arrival estimation using reconfigurable antennas," in *Proc. IEEE 27th Can. Conf. Electr. Comput. Eng. (CCECE)*, May 2014, pp. 1–4.
- [26] H. Paaso, A. Mammela, D. Patron, and K. R. Dandekar, "Modified MUSIC algorithm for DOA estimation using CRLH leaky-wave antennas," in *Proc. 8th Int. Conf. Cognit. Radio Oriented Wireless Netw.*, Jul. 2013, pp. 166–171.
- [27] C. Plapous, J. Cheng, E. Taillefer, A. Hirata, and T. Ohira, "Reactance domain MUSIC algorithm for electronically steerable parasitic array radiator," *IEEE Trans. Antennas Propag.*, vol. 52, no. 12, pp. 3257–3264, Dec. 2004.
- [28] M. Li, R. Ma, and N. Behdad, "A compact, low-cost, ultrawideband direction-finding system: Techniques suitable for small-aperture designs," *IEEE Antennas Propag. Mag.*, vol. 60, no. 6, pp. 32–44, Dec. 2018.
- [29] M. I. Jais, T. Sabapathy, M. Jusoh, R. Badlishah Ahmad, M. H. Jamaluddin, M. R. Kamarudin, P. Ehkan, L. M. Loganathan, and P. J. Soh, "A fuzzy-based angle-of-arrival estimation system (AES) using radiation pattern reconfigurable (RPR) antenna and modified Gaussian membership function," *IEEE Access*, vol. 7, pp. 145477–145488, 2019.
- [30] A. Cidronali, G. Collodi, S. Maddio, M. Passafiume, G. Pelosi, and S. Selleri, "Improving phaseless DoA estimation in multipath-impaired scenarios by exploiting dual-band operations," in *IEEE MTT-S Int. Microw. Symp. Dig.*, May 2016, pp. 1–4.
- [31] X. Wang and E. Aboutanios, "Reconfigurable adaptive linear array signal processing in GNSS applications," in *Proc. IEEE Int. Conf. Acoust., Speech Signal Process.*, May 2013, pp. 4154–4158.
- [32] T. G. Dvorkind and E. Greenberg, "DOA estimation and signal separation using antenna with time varying response," in *Proc. 22nd Eur. Signal Process. Conf. (EUSIPCO)*, Sep. 2014, pp. 1039–1043.
- [33] M. Rzymowski, K. Trzebiatowski, K. Nyka, and L. Kulas, "DoA estimation using reconfigurable antennas in millimeter-wave frequency 5G systems," in *Proc. 17th IEEE Int. New Circuits Syst. Conf. (NEWCAS)*, Jun. 2019, pp. 1–4.
- [34] R. Schmidt, "Multiple emitter location and signal parameter estimation," *IEEE Trans. Antennas Propag.*, vol. 34, no. 3, pp. 276–280, Mar. 1986.
- [35] W. Lin and H. Wong, "Multipolarization-reconfigurable circular patch antenna with L-shaped probes," *IEEE Antennas Wireless Propag. Lett.*, vol. 16, pp. 1549–1552, 2017.
- [36] Y. M. Pan, K. W. Leung, and L. Guo, "Compact laterally radiating dielectric resonator antenna with small ground plane," *IEEE Trans. Antennas Propag.*, vol. 65, no. 8, pp. 4305–4310, Aug. 2017.
- [37] W. Lin and R. W. Ziolkowski, "Electrically small Huygens antenna-based fully-integrated wireless power transfer and communication system," *IEEE Access*, vol. 7, pp. 39762–39769, 2019.
- [38] H. L. Van Trees, *Optimum Array Processing (Part IV of Detection, Estimation, and Modulation Theory)*. New York, NY, USA: Wiley, 2002.
- [39] M. Eric, A. Zejak, and M. Obradovic, "Ambiguity characterization of arbitrary antenna array: Type I ambiguity," in *Proc. IEEE 5th Int. Symp. Spread Spectr. Techn. Appl.-Spread Technol. Afr.*, vol. 2, Sep. 1998, pp. 399–403.
- [40] M. J. D. Rendas and J. M. F. Moura, "Ambiguity in radar and sonar," *IEEE Trans. Signal Process.*, vol. 46, no. 2, pp. 294–305, Feb. 1998.
- [41] D. Rodrigo, Y. Damgaci, N. Biyikli, B. A. Cetiner, J. Romeu, and L. Jofre, "MEMS-reconfigurable antenna based on a multi-size pixelled geometry," in *Proc. 4th Eur. Conf. Antennas Propag.*, Apr. 2010, pp. 1–4.
- [42] X. Yuan, Z. Li, D. Rodrigo, H. S. Mopidevi, O. Kaynar, L. Jofre, and B. A. Cetiner, "A parasitic layer-based reconfigurable antenna design by multi-objective optimization," *IEEE Trans. Antennas Propag.*, vol. 60, no. 6, pp. 2690–2701, Jun. 2012.
- [43] Z. Li, D. Rodrigo, L. Jofre, and B. A. Cetiner, "A new class of antenna array with a reconfigurable element factor," *IEEE Trans. Antennas Propag.*, vol. 61, no. 4, pp. 1947–1955, Apr. 2013.
- [44] T. Sabapathy, M. F. Jamlos, R. B. Ahmad, M. Jusoh, and M. I. Jais, "A reconfigurable microstrip rectangular parasitic array antenna," in *Proc. IEEE Symp. Wireless Technol. Appl. (ISWTA)*, Sep. 2013, pp. 372–375.



BRAD R. JACKSON (Senior Member, IEEE) received the B.Sc.(Eng.), M.Sc.(Eng.), and Ph.D. degrees in electrical engineering from Queen's University, Canada, in 2002, 2005, and 2009, respectively.

From 2009 to 2010, he was a Postdoctoral Fellow at the Royal Military College of Canada, where he conducted research on antennas and radar systems. From 2010 to 2017, he was a Defence Scientist at the Defence Research and Development Canada, where he conducted research on communications electronic warfare. He is currently an Assistant Professor at the Department of Electrical and Computer Engineering, California State University, Northridge. He has published over 40 peer-reviewed papers in the areas of RF/microwave circuits, antennas, and electronic warfare. His research interests include smart antennas, broadband and reconfigurable antennas, direction of arrival estimation, electronic warfare, and RF/microwave circuits.

• • •